

Journal of Materials Chemistry A

Accepted Manuscript



This is an *Accepted Manuscript*, which has been through the Royal Society of Chemistry peer review process and has been accepted for publication.

Accepted Manuscripts are published online shortly after acceptance, before technical editing, formatting and proof reading. Using this free service, authors can make their results available to the community, in citable form, before we publish the edited article. We will replace this *Accepted Manuscript* with the edited and formatted *Advance Article* as soon as it is available.

You can find more information about *Accepted Manuscripts* in the [Information for Authors](#).

Please note that technical editing may introduce minor changes to the text and/or graphics, which may alter content. The journal's standard [Terms & Conditions](#) and the [Ethical guidelines](#) still apply. In no event shall the Royal Society of Chemistry be held responsible for any errors or omissions in this *Accepted Manuscript* or any consequences arising from the use of any information it contains.

Cite this: DOI: 10.1039/c0xx00000x

www.rsc.org/xxxxxx

Engineered graphene-nanoparticle aerogel composites for efficient removal of phosphate from water

Diana N.H. Tran, Shervin Kabiri, Luoshan Wang, and Dusan Losic*

Received (in XXX, XXX) Xth XXXXXXXXX 20XX, Accepted Xth XXXXXXXXX 20XX

DOI: 10.1039/b000000x

The contamination of aqueous systems with phosphates has considerable environmental concerns and here, we present a new method for phosphate removal based on graphene aerogel composites. 3-dimensional graphene aerogels decorated with goethite (αFeOOH) and magnetite (Fe_3O_4) nanoparticles were synthesised and their application for capturing phosphates in water was successfully demonstrated. The prepared aerogels showed superior capacity to remove up to 350 mg/g at an initial phosphate concentration of 200 mg/L from water. The Freundlich model was suitable to describe the adsorption mechanism of phosphate removal by the graphene-iron nanoparticle aerogels through both mononuclear and polynuclear adsorption onto the nanosized αFeOOH and Fe_3O_4 nanoparticles. These new phosphate adsorbents can be produced in different forms and dimensions, using a simple, green and scalable process, and have potential to be applied for practical applications for phosphate management of waste and storm waters.

Introduction

Phosphate is an essential nutrient for the growth of many living organisms, both on land and in the aquatic environment. However, the need for restoring nutrients to the land and the increased demand for food from a growing population has led to the development and widespread use of artificial fertilisers. As a result of agricultural production and human consumption (detergent and other high-grade applications), this has caused an excessive amount of phosphate in the water, therefore deteriorating the quality of water.¹ Hence, the challenge to recover, recycle and/or remove phosphate (expressed as P_2O_5) from wastewater and environmental waters is recognised as an important problem for industry (fertilisers, phosphorous chemicals, etc.) and for environmental engineers to find efficient and cost effective technology. Many technologies have been developed for the removal of phosphorous from wastewater including chemical precipitation, biological treatment, membrane processes, adsorption, ion exchange and crystallisation.²⁻⁵ Chemical precipitation based on metal salts such as, calcium (Ca), iron (Fe), and aluminium (Al) is usually

applied to remove phosphate in the secondary wastewater treatment. It is suggested that aluminium sulphate (Al_2SO_4) is the best precipitant, followed by Fe(III), Fe(II) and finally Ca for the removal of phosphate.⁶ These materials are available as solid waste from other processes and can be used as low-cost or free source for the development of phosphate adsorbents at an industrial scale. Red mud (RM) is a waste residue of alumina refinery, which mainly composes of fine particles containing aluminium oxide (Al_2O_3), iron oxide (Fe_2O_3), silica (SiO_2), titanium oxides and hydroxides.⁷ Similarly, steel slags (composed of Fe_2O_3 , calcium oxide (CaO) and SiO_2) produced from industrial by-products has also been used to remove phosphate from synthetic solutions and real wastewater.⁸ Previous studies from Yeoman et al.² showed that Fe(III) has greater affinity for phosphate than Fe(II) as the salt most commonly used in wastewater treatment is iron(III) chloride (FeCl_3). Fe(II) ions can only be used if they are first oxidised to the Fe(III) form, whereas Fe(III) ions form strong complexes with pyrophosphate and tripolyphosphates.^{9,10} However, chemical precipitation generates unwanted chemicals and waste disposal issues, which is unfavourable.

Common biological treatments use activated sludge in the secondary wastewater treatment plant during the biological nutrient removal process. Although it is efficient for the removal of nitrite, the removal of phosphate is relatively low.² However, the drawback of biological treatment is there still needs to be a primary biological treatment and is prone to operational difficulties.³

Adsorption methods based on different adsorbents, such as

* School of Chemical Engineering, The University of Adelaide, Adelaide, SA 5005, Australia. E-mail: dusan.losic@adelaide.edu.au

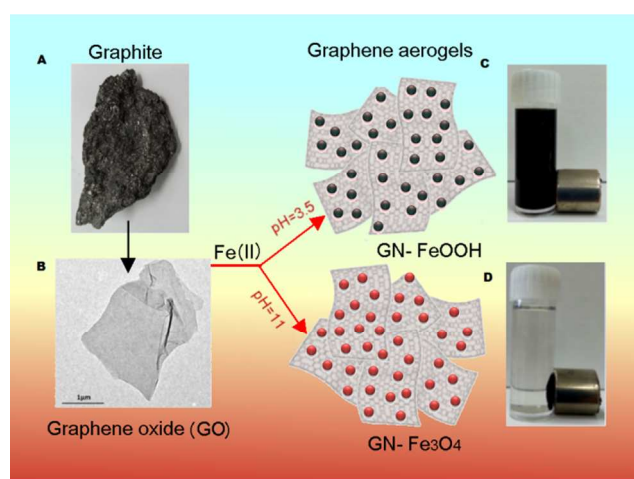
† Electronic Supplementary Information (ESI) available: See DOI: 10.1039/b000000x/

natural pumice powders, bauxite refinery residues (BauxsolTM), and farm effluents have been explored and practically implemented.¹¹⁻¹³ Adsorbents based on bare activated carbon (AC) have also been proven to be an effective adsorbent for other hazardous contaminants in water, but did not show to be very effective for phosphate removal.^{14,15} It has been shown that a pre-oxidation treatment for AC can increase the amount of Fe impregnation in the carbon, and therefore enhance the adsorption of phosphate. From the different types of oxidants (potassium permanganate, hydrogen peroxide, sulphuric and nitric acid) evaluated, the results indicated that nitric acid was the best oxidiser for the pre-oxidation treatment of AC, and iron sulphate (FeSO₄) was the most suitable iron salt for phosphate removal, compared to FeCl₃. The 34-46.6 % higher phosphate removal efficiency demonstrated here suggests that functionalised high surface area carbon materials is a feasible strategy to design advanced adsorbents for phosphate removal.¹⁶ Metal oxide materials with high surface area based on high affinity for phosphate area were recently explored as an alternative approach showing excellent adsorption performance.¹⁷⁻¹⁹

Graphene, the latest member of the carbon family, has proved itself to be an excellent adsorbent for environmental and water remediation.²⁰⁻²² It has drawn significant attention in research and industry due to its unique physical, chemical, mechanical and electrical properties not seen before in other carbon materials.^{23,24} Graphene and graphene oxide (GO) due to its enormous surface area (> 2000 m²/g) have shown outstanding adsorption performance due to strong π - π interaction with organic molecules or oxygen groups for metal ions that plays an important role for their adsorption properties.²¹ Graphene and GO have been explored for adsorption of many environmental pollutants including, oil, heavy metals, dyes, and organics. Surprisingly not many studies are reported for application of graphene based adsorbents for phosphate removal. The most recent study showed that micrometre graphene sheets prepared from exfoliated graphite was an effective adsorbent for the adsorption/removal of phosphate from aqueous solution.²⁵ The adsorption capacity of 89.37 mg/g is demonstrated which is comparable with AC and metal oxide based adsorbents that suggests the potential of graphene based adsorbents. However, the reported method is not optimised for practical applications, and could cause additional environmental pollutions because of the potential release of graphene particulates in the water. In our previous work, we demonstrated that graphene aerogel composites in the form of unique 3-dimensional (3-D) structures is an excellent solution for designing advanced adsorbents for oil, mercury, and arsenic removal from water.^{26,27} To our knowledge there is no study on the adsorption of phosphate using graphene-based aerogels with embedded nanoparticles, especially for magnetic particles, which we present here.

The aim of this work is to demonstrate for the first time the application of graphene-based materials in the form of aerogels for adsorption of phosphate from water. The synthesis was performed using a simple, green synthetic method from graphite as a natural and low cost source, which is widely available from the mining industry. Fe nanoparticles are embedded into the graphene during the reduction process of GO to increase the adsorption capacity and efficiency of the material that is proved

in previous studies. Scheme 1 shows the preparation of the 3-D graphene-Fe nanoparticles (GN-Fe) aerogel composite. The significance of this method is that it requires only a one-step synthesis approach without the use of any hazardous compounds, generally required for the reduction of GO. Two types of Fe material (α -FeOOH and magnetic Fe₃O₄) are produced depending on the pH conditions (i.e. acidic and basic) in order to explore their adsorption properties toward phosphate ions. The deposited Fe nanoparticles (NPs) on the graphene sheets also act as spaces that effectively stop the aggregation of the graphene sheets during the reduction. The formed 3-D hydrogel is finally transformed into an aerogel by freeze drying to form a graphene aerogel embedded with Fe nanoparticles. The prepared graphene aerogel composites were characterised to confirm their structure, chemical composition, phosphate adsorption performance, kinetics, and possible reaction mechanism involved in the removal of phosphate from water.



Scheme 1. A schematic diagram illustrating the formation of graphene-Fe aerogels through hydrolysis and co-precipitation. (a) Graphite ore, (b) graphene oxide (GO) sheet, (c) graphene- α FeOOH (GN- α FeOOH) aerogels fabricated at low pH, and (d) graphene-Fe₃O₄ (GN-Fe₃O₄) aerogels fabricated at high pH. Photographs in (c) and (d) represent the magnetic separation of GN- α FeOOH and GN-Fe₃O₄ aerogels from solution, respectively.

Experimental part

Materials and chemicals

Natural graphite flakes were supplied by a local mining site (Uley, Eyre Peninsula, South Australia) that were milled into a fine powder using a bench top ring mill (Rocklabs). Iron sulphate (FeSO₄·7H₂O) and potassium permanganate (KMnO₄) was purchased from Sigma-Aldrich, Australia. Sulphuric acid (H₂SO₄, 98 %), phosphoric acid (H₃PO₄, 85 % w/w), hydrogen peroxide (H₂O₂, 30 %), hydrochloric acid (HCl, 35%), sodium hydroxide (NaOH), ammonium solution (NH₄OH, 30 %), monopotassium phosphate (KH₂PO₄) and ethanol were purchased from Chem-Supply, Australia. All chemicals were used directly without further processing. High-purity Milli-Q water (18.2 M Ω) was used throughout the study, unless otherwise stated.

Preparation of graphene oxide (GO)

Graphene oxide sheets were synthesized by the improved

Hummer's method from the natural graphite.²⁸ 3 g of graphite powder and 18 g of KMnO₄ were slowly mixed at room temperature with a 9:1 mixture of concentrated H₂SO₄ and H₃PO₄ (360:40 mL), which was previously kept at 4°C for 3-4 h. Under constant stirring, the mixture was then placed in a silicon oil bath and heated to 50 °C for approx. 12 h to form a thick paste. The reaction was cooled to room temperature and poured onto ice (450 mL) with 3 mL of H₂O₂. The mixture was then washed twice with distilled (DI) water, once with HCl (32 %), and then twice again with ethanol until a light brown product was obtained, which were GO sheets. Each sequential wash was centrifuged at 4200 rpm for 2 h where the supernatant was discarded. The obtained GO was dried overnight in a 45 °C oven and characterised with Raman and TGA.

15 Preparation of GO Synthesis of Graphene- α FeOOH (GN- α FeOOH) and Graphene-Fe₃O₄ (GN-Fe₃O₄) Aerogel Composites

Graphene-Fe aerogel composites were synthesized according to the literature.²⁹ 40 mg of GO (2 mg/mL) was dissolved in water with 1 mmol of FeSO₄. For graphene- α FeOOH aerogels, the GO suspension was adjusted to pH 3-3.5 with HCl, whereas for the graphene-Fe₃O₄ aerogels the pH was adjusted to 11 with NH₄OH. The glass vials were then placed in a 90 °C silicon oil bath for 6-8 h without stirring. After the reaction, the 3-D black hydrogels were taken out and washed with DI water, and freeze dried for 24 h to obtain a porous and light weighted aerogel.

Characterisations

The prepared materials including graphite, GO, and graphene-Fe aerogels (GN- α FeOOH and GN-Fe₃O₄) were characterised by several analytical techniques such as, scanning electron microscopy (FE-SEM, Quanta 450, FEI, USA), transmission electron microscopy (TEM, Tecnai G2 Spirit, FEI, USA), optical microscopy (Leica MZ16FA Stereo, Leica Microsystems, Australia), light scattering (Mastersizer 2000, Malvern, Australia), Fourier transform infrared (FTIR) spectroscopy (Spectrum 100, Perkin Elmer, USA), Raman spectroscopy (LabRAM Evolution, Horiba Jvon Yvon, Japan), X-ray diffraction (XRD, Miniflex 600, Rigaco, Japan) and Thermogravimetric analyser (TGA, Q500, TA Instruments, USA).

SEM was conducted to confirm the structure and morphology of GO and GN-Fe aerogels. The GN-Fe aerogels were also analysed by TEM to confirm the attachment of α FeOOH nanorods and magnetic Fe₃O₄ nanoparticles onto the reduced GO surface operating at an accelerating voltage of 100 kV. Samples were prepared by sonicating the aerogels in ethanol for 60 minutes and then drop casting the suspension on a Lacey copper grid for analysis. FTIR characterisation of these samples was performed to further support the reduction of GO to GN by Fe. All spectra were collected in the range of 4000-500 cm⁻¹ in transmission mode. XRD measurement was collected to illuminate the composition of GO and GN-Fe aerogels at 40 kV and 15 mA in the range of 2 θ = 10-80° with a scan speed of 6 °/min. Furthermore, to investigate the graphitic structure of GO before and after the aerogel synthesis, the samples (i.e. graphite, GO, GN-Fe aerogels) were analysed by Raman spectroscopy using a 532 nm laser (mpc 3000) as the excitation source. A 100x

objective was used with a confocal size of 300 μ m. The laser power was kept at or below 50 %. A scan was collected for each sample in the spectral range of 500-3500 cm⁻¹ using an integration time of 10 s for 3 accumulations. Samples were deposited on glass slides in solid form without any solvent. All spectra shown are from raw and unprocessed data. Thermal decomposition of GO and graphite was performed by thermal gravimetric analyser (TGA) under nitrogen atmosphere where the samples were heated to 1000 °C at a heating rate of 10 °C/min. Optical images of the graphite flakes were taken with the 100x objective under a white light source. Particle size distribution (PSD) was also collected for the graphite in DI water. An average of three measurements was taken. In addition, the specific surface areas (SSA) of the GN-Fe aerogels were determined by the methylene blue (MB) adsorption method by UV-Vis spectroscopy (Shimadzu UV-1601, Japan).^{30,31} A known mass of the aerogel was placed into a known volume MB solution of standard concentration (i.e. 20 mg/L). The suspension was sonicated for 2 h and then continuously stirred for 24 h to reach the adsorption-desorption equilibrium of MB. An aliquot was taken from the suspension and centrifuged to remove any suspended material. The MB concentration was determined by measuring the supernatant with UV-Vis at a wavelength of 665 nm compared with the initial standard concentration. The SSA can be calculated from the amount of adsorbed MB according to the following equation:

$$85 \quad SSA = \frac{N_A A_{MB} (C_0 - C_e) V}{M_{MB} m_s} \quad (1)$$

where N_A represents Avogadro number (6.02×10^{23} /mol), A_{MB} (m²) is the covered area of per MB molecules (typically assumed to be 1.35 nm²), V (L) is the volume of MB solution, M_{MB} (g/mol), is the relative molecular mass of MB, m_s (g) is the mass of the sample, and C_0 (mg/L) and C_e (mg/L) are the initial and equilibrium concentrations of MB, respectively.

Batch Adsorption Experiments

Adsorption experiments were conducted by varying contact time, pH and initial phosphate concentration for adsorption isotherms and kinetics studies. Phosphate solutions of 50 mL (used KH₂PO₄) with different initial concentrations (10-500 mg/L) were mixed with 10 mg of GN-Fe aerogels at ambient temperature. The mixtures were then stirred continuously for 24 h to reach equilibrium. A sample (1 mL) of the mixtures was then withdrawn in 1.5 mL Eppendorf tubes and centrifuged at 14,200 rpm for 10 min and the supernatant was collected and prepared for solution Inductively coupled plasma-mass spectrometry (ICP-MS 7500 cs, Agilent Technologies).

For effect of pH, the experiments were performed similarly to the aforementioned procedure but with 100 mL phosphate solutions (20 mg/L) mixed with 10 mg of the adsorbent. The mixtures were also stirred for 24 h to reach equilibrium before removing, centrifuging and prepared for ICP analysis. Experiments were performed in the range of pH 2 to 10 using HCl and NaOH (1 M). All the experiments were performed in duplicates. The amount of phosphate adsorbed onto the GN-Fe aerogels, q_e (mg/g), was calculated by the following equation:

$$q_e = \frac{(C_0 - C_e)V}{m_s} \quad (2)$$

where C_0 (mg/L) and C_e (mg/L) are the initial and equilibrium concentrations of phosphate, respectively; V (L) is the solution volume, and m_s is the mass of the adsorbent.

The kinetic studies were performed at ambient temperature with the initial phosphate concentration set as 20 mg/L. The mixture was continuously stirred and samples were taken at predetermined time intervals from 0 to 3 h. The residual phosphate concentration was analysed by the same method described above. Each experiment was carried out in triplicates under identical conditions.

Results and Discussion

Characterisation of prepared GO

A SEM image of the graphite flakes used as the source for exfoliation of GO in this work is presented in Fig. 1a. The image shows that the graphite is irregular in shape with different sizes from 100–300 μm (PSD not shown). The typical structural morphology of the prepared GO sheets was analysed by TEM (Fig. 1a (bottom)) which confirmed the paper-like sheet of the GO. The graphitic structure of GO was confirmed by Raman spectroscopy (Fig. 1b) showing the characteristic D and G bands at [1250–1450] cm^{-1} and [1550–1650] cm^{-1} , respectively. The D band indicates the structural defects and disorder, whereas the G band represents the graphitic component in the structure.³² The higher D band intensity and weak 2D band suggests the presence of structural defects of the GO (low sp^2 domains) and the presence of imperfections in the form of hydroxyl and epoxy groups on its basal planes.³³

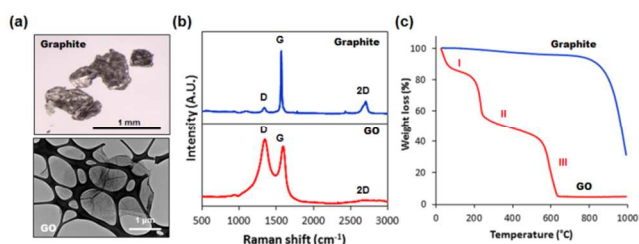


Figure 1. (a) An optical image of graphite flakes (top) and a TEM image of GO sheet (bottom) prepared by the aforementioned process, (b) Raman spectra of GO and graphite showing G, D and 2D bands, and (c) TGA spectra of graphite and GO. The deoxygenation process of GO is illustrated by phase I, II and III.

On the other hand, graphite shows a characteristic primary peak around 1570 cm^{-1} (G band) and a prominent peak around 2700 cm^{-1} (2D) that is not observed in GO. This is due to the planar sp^2 bonded carbon atoms, and two phonon lattice vibrations in the graphitic structure, respectively. Thermogravimetric analysis (TGA) of graphite and exfoliated GO was collected as a function of temperature and shown in Fig. 1c. The results show that graphite was highly stable up to 800 $^{\circ}\text{C}$ as expected. While GO showed decrease in mass from room temperature to 200 $^{\circ}\text{C}$ (region I), which are associated with the loss of water molecules. The second major mass loss after 200 to 600 $^{\circ}\text{C}$ (region II) was caused by pyrolysis of the oxygen-containing functional groups

generating carbon monoxide (CO), carbon dioxide (CO_2) and steam as by-products of the reduction process. Above 600 $^{\circ}\text{C}$, the mass of GO further decreased due to the decomposition of oxygen species (region III).³⁴

Characterisation of Graphene-Fe Aerogel Composites (GN- αFeOOH and GN- Fe_3O_4)

Photographs of the prepared GN- αFeOOH and GN- Fe_3O_4 aerogels obtained after freeze drying of the hydrogels are presented in the insets of Fig. 2a and 2d. Both aerogels are black due to the reduction of GO to graphene and the rectangular shape is controlled by the mold where the reaction was carried out. SEM images of the prepared GN- αFeOOH aerogel by the hydrolysis method shows a well-defined 3-D network-like graphene structure decorated with αFeOOH nanorods, as clearly observed from the high magnification SEM and TEM images (Fig. 2b and 2c). Graphene sheets tend to agglomerate and irreversibly restack due to strong π - π and van der Waals interaction. The simultaneous reduction of GO and the distribution of metallic nanoparticles sitting on the graphene sheets prevents their restacking and agglomeration.^{35,36} The deposition of the αFeOOH nanorods on the graphene sheets induced by ferrous ions, which was used as a reducing agent to reduce the GO sheets under acidic conditions eliminates the agglomeration of the graphene sheets during the reduction process. Similarly, an interconnected network structure with micrometer pore sizes is seen for the GN- Fe_3O_4 aerogel (Fig. 2d) as the iron nanoparticles act as spacers between the graphene sheets. The walls of the self-assemble graphene sheets appear slightly thicker probably due to the cluster of Fe_3O_4 nanoparticles deposited on both sides of the sheet (Fig. 2e). Fig. 2f shows a typical TEM image of the nanoparticles on the surface of the graphene wall in the aerogel.

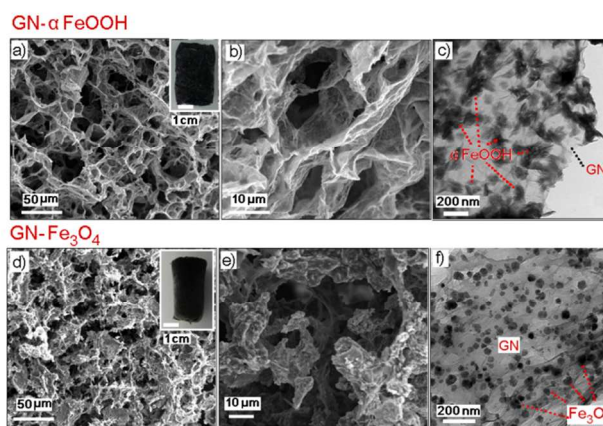


Figure 2. SEM images of a GN- αFeOOH and GN- Fe_3O_4 aerogels at (a, d) low and, (b, e) high magnification, respectively. TEM images of (c) αFeOOH nanorods and, (f) magnetic Fe_3O_4 nanoparticles on graphene sheets. Insets in (a) and (d) show photos of the prepared graphene-Fe aerogels (GN- αFeOOH and GN- Fe_3O_4 , respectively) with dimensions 1.5–2 cm diameter and 3–4 cm in length.

These magnetite (Fe_3O_4) nanoparticles have an average diameter of 45 nm and are randomly distributed on the surface of the graphene sheets. They are formed by co-precipitation with the aid of the ammonium solution. At low pH, the existence of abundant

polar oxygen-containing groups on the GO sheets such as epoxy, carboxyl, and hydroxyl can induce diffusion of ferrous (Fe^{2+}) ions toward the GO sheets by electrostatic interaction, which is oxidized into ferric (Fe^{3+}) ions by the oxygen containing groups on the surface of GO. αFeOOH nanorods is formed on the reduced GO surface simultaneously by the hydrolysis of Fe^{3+} ions (Scheme 1c). However, at high pH the oxidised Fe^{2+} and Fe^{3+} ions will co-precipitate into magnetic Fe_3O_4 nanoparticles (Scheme 1d), as previously reported.^{29,37,38}

Fig. 3a shows the XRD profiles of the GN- αFeOOH (2) and GN- Fe_3O_4 aerogels (3) compared to GO (1) used as the control. The large broad peak observed in GO is typical of amorphous materials with no crystallites. The peak at $2\theta = 25.4^\circ$ corresponds to the (002) plane of the graphitic structure of GO, which indicates an incomplete oxidation of GO.^{39,40} However, this peak disappears after being reacted with FeSO_4 , therefore GO is reduced by FeSO_4 .^{29,41-43} The diffraction peaks for GN- αFeOOH aerogel, at 16.16, 17.94, 23.6, 27.4, 32.84, 36.66, 38.9, 52.98, and 58.4° , correspond to the (020), (110), (120), (310), (130), (111), (140), (221) and (151) planes of the crystalline iron species goethite (αFeOOH) (PDF card no. 9003076); while, all the peaks up to $2\theta = 23.4^\circ$ of the GN- Fe_3O_4 aerogel can be assigned to magnetite (Fe_3O_4) (PDF card no. 9005814). The magnetic property of the GN- Fe_3O_4 aerogel is also confirmed when the material was separated from the solution by a magnet (Scheme 1d) leaving clear water behind, unlike the GN- αFeOOH dispersion, which was still black (Scheme 1c). FTIR plots of GO (1) and both the prepared GN-Fe aerogels are shown in Fig. 3b. Several characteristic peaks are observed for GO: OH ($\sim 3340\text{ cm}^{-1}$), C=O ($\sim 1742\text{ cm}^{-1}$), C=C ($\sim 1634\text{ cm}^{-1}$), and C-O (~ 1210 and 1020 cm^{-1}). The FTIR spectra of the GN- αFeOOH (2) and the GN- Fe_3O_4 aerogels (3) show slight changes in the characteristic peaks from 1740 to 1200 cm^{-1} . There is an obvious decrease in the oxygen functional groups of the carbonyl and epoxy, indicating the effective reduction of the GO sheets. Although, a significant increase of the adsorption peak at $\sim 1070\text{ cm}^{-1}$ (C-O) is still observed in the reduced GO (rGO) sheets. This is because only some of the sp^3 bonded carbon in GO is converted to sp^2 bonded carbon during the reduction process and the structure of graphene is seldom fully recovered in rGO.⁴⁰ Meanwhile, the two bands at 905 and 795 cm^{-1} in the GN- αFeOOH aerogel can be assigned to the Fe-O-H bending vibrations in αFeOOH .³⁰ In addition, the absorption peak at 645 and 580 cm^{-1} is indicative of the existence of magnetite in the GN- Fe_3O_4 aerogels.⁴⁴

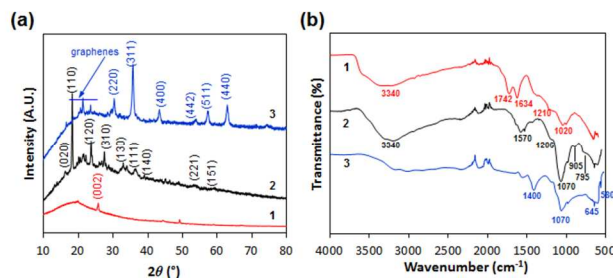


Figure 3. (a) XRD and (b) FTIR plots of GO (1), GN- αFeOOH aerogel (2) and GN- Fe_3O_4 aerogel (3), respectively.

Furthermore, Raman characterisation of the GN-Fe aerogels

prepared by both the hydrolysis and coprecipitation method shown in Fig. 4 provides evidence for the attachment of Fe onto the reduced GO sheets. The intensity ratio of the D and G band (I_D/I_G) is a useful indicator to evaluate the ordered or disordered crystal structures of carbon. Raman analysis of the GN- αFeOOH and GN- Fe_3O_4 samples both showed a slight increase in I_D/I_G of the D and G bands of graphene in the aerogels (0.84 and 0.85), respectively, compared with that for GO (0.83), confirming the increasing disordered graphene sheets.³¹ The peak shifts in the D and G bands of the aerogel also reveals the charge transfer between the graphene sheets and αFeOOH nanorods,³⁸ and Fe_3O_4 nanoparticles.³⁷ In addition, the Raman band at 580 cm^{-1} is in agreement with the FTIR results for the existence of magnetite. Hence, it can be concluded from the above analyses that the GN- αFeOOH aerogel formation is by the coassembly of graphene sheets and αFeOOH nanorods through the reduction of GO to graphene by Fe^{2+} and the hydrolysis of Fe^{3+} ions. While, the GN- Fe_3O_4 aerogel is formed by the anchoring of $\text{Fe}^{2+}/\text{Fe}^{3+}$ on COO^- groups on the GO sheets, the Fe_3O_4 nanoparticles were formed by coprecipitation with the addition of ammonium solution. The in situ simultaneous deposition of metal oxide nanoparticles and the self-assembly of GO sheets into the 3-D interconnected hydrogel structure is also driven by the combined hydrophobic and π - π stacking interactions, due to the reduction of oxygenated moieties on the graphene surface. In addition, the precipitated nanoparticles effectively served as spacers to eliminate the agglomeration of the graphene sheets during the reduction process.⁴⁵

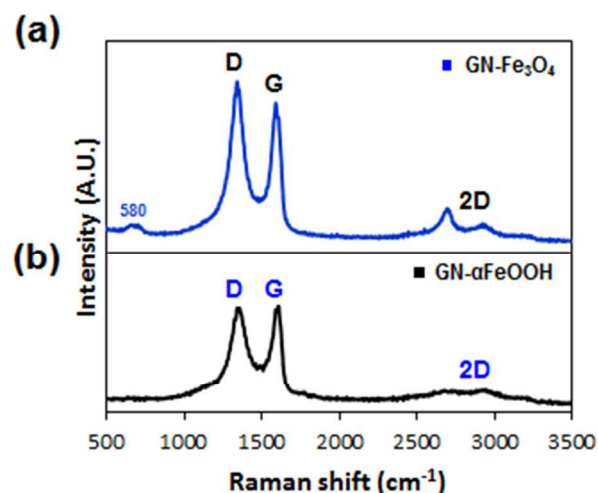


Figure 4. Raman plots of (a) GN- αFeOOH aerogel and (b) GN- Fe_3O_4 aerogel.

Adsorption Kinetics

Typical adsorption curves for the removal of phosphate by both types of graphene-Fe nanoparticle aerogels using a model solution with 20 mg/L phosphate concentration is presented in Fig. 5. This figure shows a very fast adsorption process of approx. 50-60 % phosphate removal within the first 5 min and then a steady 80 % removal within 1 h.

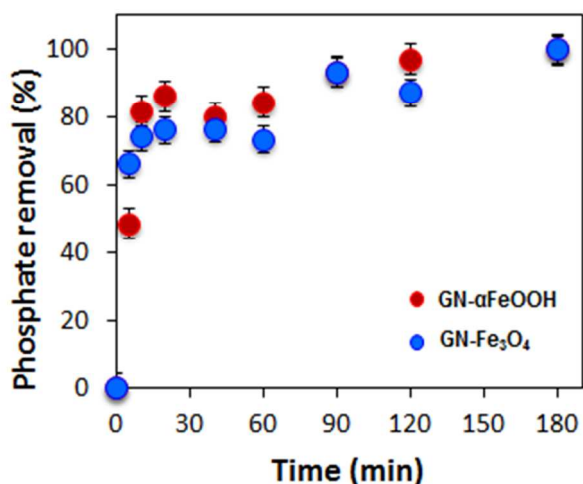


Figure 5. The effect of time on the amount of phosphate adsorbed on the GN- α FeOOH and GN-Fe₃O₄ aerogels. Conditions: phosphate concentration = 20 mg/L; pH = 6.0.

To understand the mechanism of the phosphate adsorption onto the adsorbents mathematical models are used. The adsorption kinetic parameters were determined by using two models to fit the experimental results (Fig. 5), which are summarized below in Eqns. 3 and 4.⁴⁶

Pseudo first-order equation

$$\log(q_e - q_t) = \log q_e - \frac{k_1}{2.303} t \quad (3)$$

Pseudo second-order equation:

$$\frac{t}{q_t} = \frac{1}{k_2 q_e^2} + \frac{1}{q_e} t \quad (4)$$

where q_e and q_t are the amount of phosphate adsorbed (mg/g) at equilibrium and at time t (min), respectively, and k_1 , and k_2 , are the rate constants for the pseudo first-order and pseudo second-order kinetic models, respectively.

The equilibrium adsorption capacity and rate constants determined from the slopes of the line and intercepts of the plots for the two models are compiled in Table 1. The plots were found to be linear with good correlation coefficients. The theoretical $q_e(\text{cal})$ values for both GN- α FeOOH and GN-Fe₃O₄ aerogel composites agreed well with the experimental $q_e(\text{exp})$ values for the pseudo-second order model, whereas the lower regression values obtained from the pseudo-first order equation shows the inapplicability of this model. Regarding the maximum adsorption and rate constants from the present results, it was clear that the GN- α FeOOH aerogel displayed the highest adsorption capacity at 29.98 \pm 2 mg/g. Hence, the second order model can be used to explain the adsorption of phosphate on the graphene-iron aerogels.

Effect of pH

Generally, pH represents substantial impact on the phosphate adsorption as phosphate (P) can exist in H₃PO₄, H₂PO₄⁻, HPO₄²⁻ and PO₄³⁻ depending on the pH value.^{47,48} Fig. 6 shows the

phosphate uptake on the GN- α FeOOH and GN-Fe₃O₄ aerogels in the pH range from 2 to 10. The maximum phosphate uptakes were 34 \pm 2 mg/g and 33.5 \pm 2 mg/g for GN- α FeOOH and GN-Fe₃O₄ aerogels, respectively, at pH 2. These findings can be explained by considering the phosphate speciation and the surface charge of α FeOOH and Fe₃O₄ nanoparticles in different pH values. When the solution pH is lower than 6 the aerogel surface becomes strongly positive due to the hydroxylation of α FeOOH and Fe₃O₄ nanoparticles. Therefore, the positively charged hydroxylated aerogel surface can electrostatically attract negatively charged phosphate species to form mono-, and polynuclear complexes.⁴⁹⁻⁵¹ The low phosphate uptake in alkaline pH may be attributed to the fact that the surface charge of the adsorbent becomes more negative at higher pH, therefore causes more electrostatic repulsion to the negatively charged phosphate anions of HPO₄²⁻ and PO₄³⁻.

55

Table 1. Adsorption kinetic parameters of phosphate adsorption on GN- α FeOOH and GN-Fe₃O₄ aerogels.

Adsorbent	q_{exp} (mg/g)	First order equation			Second order equation		
		q_{cal} (mg/g)	k_1 (min ⁻¹)	R ²	q_{cal} (mg/g)	k_2 (x10 ⁻² g/mg.min ⁻¹)	R ²
GN- α FeOOH	29.98	30.12	0.023	0.898	29.57	0.499	0.996
GN-Fe ₃ O ₄	26.77	27.38	0.017	0.820	26.74	0.418	0.985

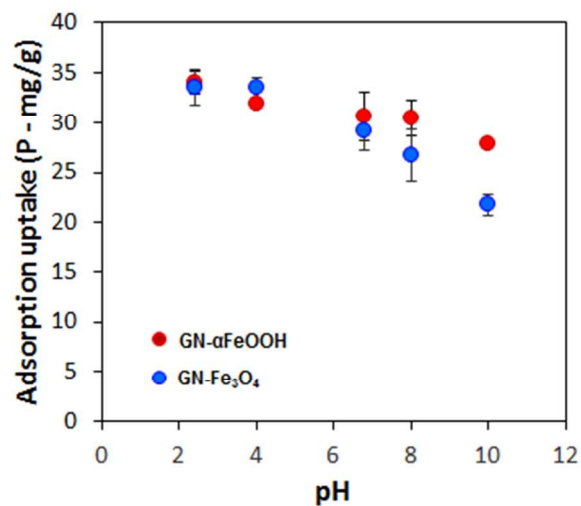


Figure 6. The effect of pH adsorbed on the amount of P adsorbed on the GN- α FeOOH and GN-Fe₃O₄ aerogels. Condition: phosphate concentration = 20 mg/L.

Adsorption isotherms

The adsorption isotherms of phosphate ions from the KH₂PO₄ solution on GN- α FeOOH and GN-Fe₃O₄ aerogels at pH = 6 are shown in Fig. 7. The maximum phosphate adsorptions were 352 \pm 5 mg/g and 311 \pm 5 mg/g for GN- α FeOOH and GN-Fe₃O₄ aerogels, respectively at approx. 200 mg/L. Interestingly, the GN- α FeOOH and GN-Fe₃O₄ aerogels showed superior phosphate sorption ability compared to most of the reported values of other carbonaceous adsorbents.^{49,53-55} Two isotherm equations (Freundlich and Langmuir) were tested to simulate the phosphate adsorption onto the GN- α FeOOH and GN-Fe₃O₄ aerogels.

75 Freundlich equation:

$$\log Q_e = \frac{1}{n} \log C_e + \log K \quad (5)$$

Langmuir equation:

$$\frac{C_e}{Q_e} = \frac{1}{bQ_{\max}} + \frac{C_e}{Q_{\max}} \quad (6)$$

where K and b represented the Freundlich affinity coefficient and the Langmuir bonding term related to their interaction energies, respectively, C_e denotes the equilibrium solution concentration of the solution, Q_{\max} is the Langmuir maximum capacity, and n is the Freundlich linearity constant. The Freundlich model is an empirical equation, which is used to describe chemisorptions onto heterogeneous surfaces with uniform energy, and no restriction to the formation of a monolayer. The Langmuir model, however, assumes monolayer adsorption onto homogeneous active sites on adsorbents.⁵⁶

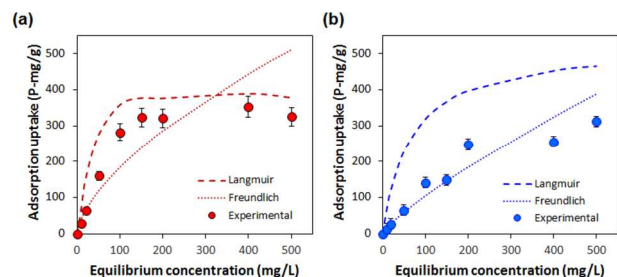


Figure 7. The adsorption isotherms of phosphate by (a) GN- α FeOOH and (b) GN- Fe_3O_4 aerogels in various KH_2PO_4 concentrations. Condition: pH = 6.0.

From Table 2, we can conclude that the regression coefficients R^2 are significantly higher for the Freundlich model ($R^2 = 0.868-0.964$) than for the Langmuir model ($R^2 = 0.595-0.866$), suggesting that the Freundlich adsorption isotherm are more suitable for the removal of phosphate by the GN- α FeOOH and GN- Fe_3O_4 aerogels. These results are consistent with the proposed predominant adsorption mechanism of phosphate removal by GN- α FeOOH and GN- Fe_3O_4 aerogels through both mononuclear and polynuclear adsorption onto the nano-sized α FeOOH and Fe_3O_4 nanoparticles. Adsorption of phosphate on iron oxides is initially fast, followed by a slow phase, which is attributed to diffusion into micropores or aggregates of particles. The adsorption of phosphate ions to iron (hydr)oxide surfaces can be described by the ligand exchange mechanism. In the adsorption process, it involves the replacement of phosphate for one or more surface hydroxyl groups, which releases surface structural OH_2 and/or OH^- into the solution.^{43,57-60} Although, the adsorption mechanism is the same for both GN- α FeOOH and GN- Fe_3O_4 aerogels, the higher phosphate adsorption capacity for GN- α FeOOH ($210 \pm 5 \text{ m}^2/\text{g}$) compared to GN- Fe_3O_4 ($130 \pm 5 \text{ m}^2/\text{g}$) aerogels can be attributed to their surface areas.¹⁶ The porous structure of the prepared aerogels is due to the α FeOOH and Fe_3O_4 nanoparticles acting as spaces in the graphene sheets. It was observed that the binding of phosphate with Fe is very strong without phosphate leaching over time. We considered several recycling strategy to weaken this binding to explore the release of phosphate, which will be presented as a separate study.

Table 2. Freundlich and Langmuir parameters for phosphate adsorption onto GN- α FeOOH and GN- Fe_3O_4 aerogels.

Adsorbent	Freundlich model			Langmuir model		
	K	1/n	R^2	Q_{\max} (mg/g)	B (L/mg)	R^2
GN- α FeOOH	9.96	0.633	0.868	588	0.006	0.595
GN- Fe_3O_4	2.46	0.814	0.964	526	0.015	0.866

Conclusions

The synthesis based on a simple and green process of graphene aerogels in the form of 3-D structures decorated with two types of iron oxide nanoparticles (α FeOOH and Fe_3O_4), and their application for removal of phosphates from water is successfully demonstrated. Prepared aerogel composites showed superior ability to remove phosphate from water over a range of pH values, especially under acidic conditions. The adsorption of phosphate follows the Freundlich isotherm, and the maximum phosphate uptake at equilibrium phosphate concentration of 200 mg/L from water is approx. 300-350 mg/g. The observed performance is significantly greater compared to other reported values using activated carbon composites and metal oxide adsorbents showing commercial potential of these new types of phosphate adsorbents. The proposed synthetic process is simple, green, and scalable to make adsorbents in different forms and dimension with ease of removal during testing, and be applied for practical applications for phosphate removal in waste and storm waters.

Corresponding Author

* School of Chemical Engineering, The University of Adelaide, Adelaide, SA 5005, Australia. Tel: +61 8 8313 4648; Email: dusan.losic@adelaide.edu.au

Acknowledgments

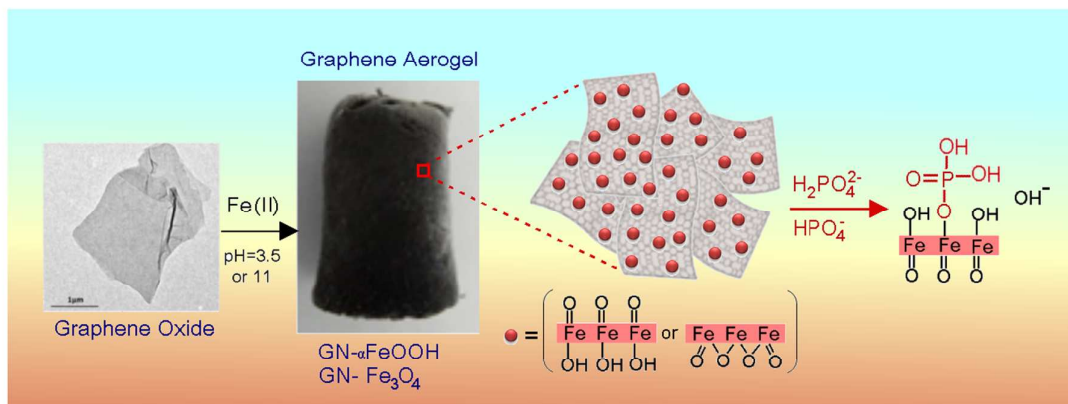
The authors acknowledge the financial support of the Australian Research Council (FT 110100711), the University of Adelaide, and Valence Industries Ltd.

References

- J. Driver, D. Lijmbach and I. Steen, *Environ. Technol.*, 1999, **20**, 651.
- S. Yeoman, T. Stephenson, J.N. Lester and R. Perry, *Environ. Pollut.*, 1988, **49**, 183.
- C.P. Leo, W.K. Chai, A.W. Mohammad, Y. Qi, A.F. Hoedley and S.P. Chai, *Water Sci. Technol.*, 2011, **64**, 199.
- P.A. Terry, *Environ. Eng. Sci.*, 2009, **26**, 691.
- E.V. Münch and K. Barr, *Water Research*, 2001, **35**, 151.
- S. Rybicki, Phosphorus removal from wastewater, A literature review, Advance Wastewater Treatment Report No. 1, 1997, Stockholm.
- W. Huang, S. Wang, Z. Zhu, L. Li, X. Yao, V. Rudolph and F. Haghseresht, *J. Hazard. Mater.*, 2008, **158**, 35.
- C. Barca, C. Gérente, D. Meyer, F. Chazarenc and Y. Andrés, *Water Research*, 2012, **46**, 2376
- D.S. Scott, Use and production of iron salts for phosphorus removal, Research Report No. 5, 1973, Canada.
- D. Jenkins, J.F. Ferguson and A.B. Menar, *Water Resources*, 1971, **5**, 369.

- 11 A.N. Onar, N. Balkaya and T. Alkyüz, *Environ. Technol.*, 1996, **17**, 207.
- 12 D.J. Akhurst, G.B. Jones, M. Clarke and D. McConchie, *Environ. Chem.*, 2006, **3**, 65.
- 13 N.S. Bolan, L. Wong and D.C. Adriano, *Bioresource Technol.*, 2004, **94**, 251.
- 14 N. Zhang, L.S. Lin and D.C. Gang, *Water Resources*, 2008, **42**, 3809.
- 15 J.K. Yang, H.J. Park, H.D. Lee and S.M. Lee, *Colloids Surf. A*, 2009, **337**, 154.
- 16 Z. Wang, M. Shi, J. Li and Z. Zheng, *J. Environ. Sci.*, 2014, **26**, 519.
- 17 J.B. Zhou, S.L. Yang, J.G. Yu and Z. Shu, *J. Hazard. Mater.*, 2011, **192**, 1114.
- 18 J. Zhang, Z. Shen, Z. Mei, S. Li and W. Wang, *J. Environ. Sci.*, 2011, **23**, 199.
- 19 K.R. Reddy, T. Xie and S. Dastgheibi, *J. Environ. Sci. Health, Part A: Toxic/Hazard. Substances Environ. Eng.*, 2014, **49**, 524.
- 20 A.K. Geim K.S. Novoselov, *Nat. Mater.*, 2007, **6**, 183.
- 21 K.C. Kemp, H. Seema, M. Saleh, N.H. Le, K. Mahesh, V. Chandra and K.S. Kim, *Nanoscale*, 2013, **5**, 3149.
- 22 D. Zhang, S. Wei, C. Kaila, X. Su, J. Wu, A.B. Karki, D.P. Young and Z. Guo, *Nanoscale*, 2010, **2**, 917.
- 23 K.P. Loh, Q. Bao, P.K. Ang and J. Yang, *J. Mater. Chem.*, 2010, **20**, 2277.
- 24 D.N.H. Tran, S. Kabiri, and D. Losic, *Carbon*, 2014, **76**, 193-202.
- 25 T-S. Jun, N-H. Park, D-S. So, J-W. Lee, K.B. Shim and H. Ham, *J. Korean Crystal Growth and Crystal Technol.*, 2013, **23**, 325.
- 26 S. Kabiri, D.N.H. Tran, T. Altalhi and D. Losic, *Carbon*, 2014, **80**, 523-533.
- 27 I. Andjelkovic, S. Kabiri, S. Azari, M. Markovic, D.N.H. Tran and D. Losic, *Carbon*, 2014, CARBON-S-14-03330 (under review).
- 28 D.C. Marcano, D.V. Kosynkin, J.M. Berlin, A. Sinitskii, Z. Sun, A. Slesarev, L.B. Alemany, W. Lu and J.M. Tour, *ACS Nano*, 2010, **4**, 4806.
- 29 H-P. Cong, X-C. Ren, P. Wang and S-H. Yu, *ACS Nano*, 2012, **6**, 2693.
- 30 M. F. El-Kady, V. Strong, S. Dubin and R. B. Kaner, *Science*, 2012, **335**, 1326.
- 31 Y. Yukselen and A. Kaya, *Eng. Geol.*, 2008, **102**, 38.
- 32 A.C. Ferrari, J.C. Meyer, V. Scardaci, C. Casiraghi, M. Lazzeri, F. Mauri, S. Piscanec, D. Jiang, K.S. Novoselov, S. Roth, and A.K. Geim, *Phys. Rev. Lett.*, 2006, **97**, 187401.
- 33 A. Kaniyoor and S. Ranprabhu, *AIP Adv.*, 2012, **2**, 032183.
- 34 A. Lerf, H. He, M. Forster and J. Klinowski, *J. Phys. Chem. B*, 1998, **102**, 4477.
- 35 M.K. Singh, E. Titus, R. Krishna, G. Goncalves, P.A.A.P. Marques, J. Gracio, *Nanosci. Nanotechnol.*, **2012**, 12, 1.
- 36 W. Choi, J-W. Lee, Graphene: Synthesis and Applications, Nanomaterials and Their Applications, CRC Press, 2012, USA.
- 37 W. Chen, S. Li, C. Chen and L. Yan, *Adv. Mater.*, 2011, **23**, 5679.
- 38 T.T. Tran, J-F. Feller, T.Y. Kim, H. Kim, W.S. Yang and K.S. Suh, *J. Polymer Sci. Part A: Polymer Chem.*, 2012, **50**, 927.
- 39 Y. Zhu, S. Murali, W. Cai, X. Li, J.W. Suk, J.R. Potts and R.S. Ruoff, *Adv. Mater.*, 2010, **22**, 3906.
- 40 T. Kuila, S. Bosa, A.K. Mishra, P. Khanra, N.H. Kim, J.H. Lee, *Prog. Mater. Sci.*, **2012**, 57, 1061.
- 41 V. Chandra, J. Park, Y. Chun, J.W. Lee, I.C. Hwang, K.S. Kim, *ACS Nano* **2010**, 4, 3979.
- 42 Q. Shou, J. Cheng, L. Zhang, B.J. Nelson, X. Zhang, *J. Solid State Chem.*, **2012**, 185, 191.
- 43 S-Y. Yoon, C-G. Lee, J-A. Park, J-H. Kim, S-B. Kim, S-H. Lee, J-W. Choi, *Chem. Eng. J.*, **2014**, 236, 341.
- 44 S. Stankovich, D.A. Dikin, R.D. Piner, K.A. Kohlhaas, A. Kleinhammes and Y. Jia, *Carbon*, 2007, **45**, 1558.
- 45 S. Nardecchia, D. Carriazo, M.L. Ferrer, M.C. Gutiérrez and F. Monte, *Chem. Soc. Rev.*, 2013, **42**, 794.
- 46 Y.S. Ho and G. Mckay, *Trans IChemE, Part B*, 1998, **76**, 332
- 47 R. Lakshmanan, C. Okoli, M. Boutonnet, S. Järäs, and G.K. Rajarao, *J. Environ. Chem. Eng.*, 2014, **2**, 185.
- 48 L. Zhang, L. Wan, N. Chang, J. Liu, C. Duan, Q. Zhou, X. Li, and X. Wang, *J. Hazard. Mater.*, 2011, **190**, 848.
- 49 Y. Yao, B. Gao, M. Inyang, A.R. Zimmerman, X. Cao, P. Pullammanappallil, and L. Yang, *J. Hazard. Mater.*, 2011, **190**, 501.
- 50 M. Zhang, B. Gao, Y. Yao, Y. Xue, and M. Inyang, *Chem. Eng. J.*, 2012, **210**, 26.
- 51 E. Kokkinos, K. Simeonidis, A. Zouboulis, and M. Mitrakas, *Desalination and Water Treatment*, 2014, 1.
- 52 R. Chirakar, S. Tezuka, A. Sonoda, K. Sakane, K. Ooi, and T. Hirotsu, *J. Colloid Interface Sci.*, 2006, **298**, 602.
- 53 Y.J. Xue, H.B. Hou, and S.J. Zhu, *J. Hazard. Mater.*, 2009, **162**, 973.
- 54 P. Kumar, S. Sudha, S. Chand, and V.C. Srivastava, *Separation Sci. Technol.*, 2010, **45**, 1463.
- 55 B.L. Chen, Z.M. Chen, and S.F. Lv, *Bioresource Technol.*, 2011, **102**, 716.
- 56 K.Y. Foo, and B.H. Hameed, *Chem. Eng. J.*, 2010, **156**, 2.
- 57 R. L. Parfitt, R.J. Atkinson, and R.St.C. Smart, *Soil Sci. Soc. Amer. Proc.*, 1975, **39**, 837.
- 58 X. Wang, F. Liu, W. Tan, W. Li, X. Feng, and D.L. Sparks, *Soil Sci.*, 2013, **178**, 1.
- 59 J.A. Arcibar-Orozco, J. Delgado-Balbuena, J.C. Rios-Hurtado, J.R. Rangel-Mendez, *Chem. Eng. J.*, **2014**, 249, 201-209.
- 60 Z. Ren, L. Shao, G. Zhang, *Water Air Soil Pollut.*, **2012**, 223, 4221-4231.

Table of Contents



The synthesis of a 3D self-assembled graphene-iron nanoparticle aerogel composite for the removal of phosphate is demonstrated with outstanding performance.